Deep Learning Assisted Printed Liquid Metal Sensory System for Wearable Applications and Boxing Training

Authors

Ye Qiu[1,2], Zhihui Zou[1], Zhanan Zou[2], Nikolas Kurnia Setiawan[2], Karan Vivek Dikshit[2], Gregory Whiting[2], Fan Yang[3], Wenan Zhang[3], Jiutian Lu[1], Bingqing Zhong[1], Huaping Wu[1]*, Jianliang Xiao[2]*

Affiliations

[1]*College of Mechanical Engineering, Zhejiang University of Technology, Hangzhou 310023, China*

[2]*Department of Mechanical Engineering, University of Colorado Boulder, Colorado, 80309, USA*

[3]*College of Information Engineering, Zhejiang University of Technology, Hangzhou 310023, China*

*To whom correspondence should be addressed.

Email:Jianliang.Xiao@colorado.edu; wuhuaping@gmaill.com

ABSTRACT

Liquid metal (LM) exhibits distinct combination of high electrical conductivity comparable to that of metals and exceptional deformability derived from its liquid state, thus it is considered a promising material for high-performance soft electronics. However, rapid patterning LM to achieve a sensory system with high sensitivity remains a challenge, mainly attributed to the poor rheological property and wettability. Here, we report a rheological modification strategy of LM and strain redistribution mechanics to simultaneously simplify the scalable manufacturing process and to significantly enhance the sensitivity of LM sensors. By incorporating SiO_2 particles into LM, the modulus, yield stress, and viscosity of the LM-SiO_2 composite are drastically enhanced, enabling 3D printability on soft materials for stretchable electronics. The sensors based on printed LM-SiO_2 composite show excellent mechanical flexibility, robustness, strain, and pressure sensing performances. Such sensors are integrated onto different locations of human body for wearable applications. Furthermore, by integrating onto a tactile glove, the synergistic effect of strain and pressure sensing can decode the clenching posture and hitting strength in boxing training. When assisted by a deep learning algorithm, this tactile glove can achieve recognition of the technical execution of boxing punches, such as jab, swing, uppercut, and combination punches, with 90.5% accuracy. This integrated multifunctional sensory system can find wide applications in smart sport-training, intelligent soft robotics, and human-machine interfaces.

Keywords: Liquid metal; Rheological modification; Strain redistribution; 3D printing; Wearable; Boxing training

1. INTRODUCTION

Liquid metals (LMs) are highly desired in skin-mounted, deformable electronics due to its distinct combination of excellent electrical conductivity comparable to that of metals and exceptional deformability derived from its liquid state[1-8]. Stretchable LM-

based flexible electronics enable precise perception of complex strain and pressure stimuli, thus holds great promise in health monitoring, advanced wearable electronics, and human-machine interfaces[9-15]. However, achieving sophisticated applications with LMs remains a daunting challenge, which requires overcoming the high surface tension of LMs and improving the sensitivity of sensors[16-21].

Recent advances in LM modification paved the way for creating better flexible electronics with improved processes[22-36]. By modifying the wetting characteristics and viscosity of LMs, the fabrication processes that originally involved lithography and reduction procedures can be simplified[37]. Some efforts have been invested to incorporate metal particles into LMs[38, 39]. To ensure homogeneous dispersion, both LMs and metal particles were acid treated to eliminate oxidation[40, 41], which allowed the particles to be wetted and suspended in the LMs to improve adhesion for directly writing on various substrates. Ultrasonic treatment has also been adopted to improve device manufacturing[42-45]. In this approach, the accelerated oxides were distributed inside LMs during sonication, to increase the viscosity of LMs. However, due to the limited viscosity improvement effect, it remains a challenge to pattern the LMs with rapid prototyping capability.

In addition to the necessity to develop an efficient preparation process, the LM-based sensors still suffer from relatively low sensitivities. Most LM-based strain sensors are based on piezoresistive effect, due to the change in electrical resistance upon deformation[46,47]. The gauge factor of a piezoresistive strain sensor attributes to two effects, the geometry change due to deformation and the resistivity change. Prior results reported that the resistivity of LMs remained unchanged due to their excellent conductivities[48-50], thus resistance change of LMs only depends on their geometry changes during deformation. The reported gauge factors of LM-based strain sensors are usually in the range of 2-6[51-53], thereby limiting their application in areas high sensitivity is required, such as skin prosthetics, humanoid robotics, and wearable health monitoring. Therefore, it is highly desirable to develop novel sensory systems based on LMs with high sensitivity.

Here, we demonstrate a modification method to modify the rheological properties

of LMs, and to enhance the sensitivity and robustness of LM-based strain and pressure sensors (Figure 1a). By mixing SiO_2 micro-particles into LM, we have effectively increased the viscosity, modulus, and yield stress, enabling the manufacturing of LM sensors through 3D printing technology. The strain redistribution mechanics tuned by SiO_2 micro-particles allows the printed sensor to achieve high sensitivity (gauge factor is 5.72 for strain range within 100%, 11.36 for 100-200%, and 23.91 for 200-300%) and excellent robustness. The sensory arrays are further integrated into a tactile glove to exploit the capability of monitoring clenching postures and punching strength in real time. Combined with a trained convolutional neural network algorithm, the multifunctional tactile glove can classify the various boxing motions, such as jab, swing, uppercut, and combination punches, with an accuracy of up to 90.5% (Figure 1b), demonstrating its capability of recognizing personal activities in boxing training.

2. RESULTS AND DISCUSSION

2.1 Rheological modification of the liquid metal

The gallium-indium alloys (Ga: In 75:25 wt%) are used as the conductive LM, and nonconductive SiO_2 particles are mixed into the LM to modify the mechanical and electrical properties (Figure S1). Two different sizes of SiO_2 particles, 40μm and 6 μm, are used for the LM composites. The rheological tests (Figures S2-S5) indicate that as the weight fraction of SiO_2 increases, the average elasticity, oscillation yield stress, shear yield stress, and the viscosity at 1 s^{-1} all increase for both LM composites (Figures 2a-2d). At the same weight ratios, the effect of rheological property modification caused by 40 μm particles is better than 6 μm particles. This is probably due to the highly viscous medium (liquid gallium indium alloy) creates a kinetic barrier to interactions among particles (Figures S6 and S7), and larger particles can overcome the barrier more easily when the ink is flowing. The increased elastic modulus, shear stress, and viscosity enable the composites to remain in shape after extrusion, rendering it 3D printable. The rheologically modified composites with 1wt.% 6 μm SiO_2 particles were used to print complicated 3D structures, such as one-layer (Figure 2e) and four-layer stars (Figure 2f), via dispensing the composites layer by layer (Videos S1 and S2). The printed conformations remain stable due to the structural support provided by the

composites, opening up new opportunities to manufacture better multifunctional stretchable electronics in an efficient way.

2.2 Characterization of the LM strain and pressure sensors

To further quantitatively evaluate the electrical and mechanical properties of the LM-SiO$_2$ microparticle composites, patterned composite wires are connected to copper tapes, and then encapsulated by Ecoflex to assemble sensing devices (Figures S8 and 3a). The strain sensor can be twisted, curled, and stretched (Figure 3b), without causing any damages to the device, demonstrating excellent mechanical flexibility and stretchability. The gauge factor of a piezoresistive strain sensor is defined as, $GF = \Delta R/(R_0\varepsilon) = (1 + 2v) + \Delta\rho/(\rho\varepsilon)$ [54-56], where ΔR is the resistance change, R_0 is the original resistance, v is the Poisson ratio, ε is the applied tensile strain, $\Delta\rho$ is the resistivity change, and ρ is the original resistivity, respectively. The theoretical relationship between the resistance change and strain indicates that increasing the strain applied to pure LM wires leads to increase in electrical resistance, which is further confirmed by the experimental measurement under uniaxial tensile strain (Figure S9). Figure 3c shows the relative resistance change of the strain sensor versus the applied tensile strain for strain sensors based on pure LM and LM-SiO$_2$ composites. For strain sensors based on pure LM, the relative resistance change shows linear increase with strain, with constant GF of 2.41. When 1 wt.% and 3.5 wt.% of 40 μm SiO$_2$ particles are mixed with the LM, the GF increases to 3.01 and 4.72, respectively. When the weight ratio of 40 μm SiO$_2$ particles increases to 6%, the curve exhibits highly nonlinear phenomenon at high strain level, leading to an effective GF of 14.65 over the strain range between 200% and 300%, which is more than six times higher than pure LM strain sensor.

To elucidate the underlying mechanism of enhanced sensitivity due to incorporation of SiO$_2$ particles, finite element analysis (FEA) is used to compare the mechanical deformation of the LM sensors. It's assumed that SiO$_2$ particles are uniformly distributed in liquid metal wires based on experimental observation (Figure S10). Figure 3d shows that the strain in the sensor based on pure LM is uniform

throughout the sensor when deformed. But for the LM sensor based on LM-SiO$_2$ composite, strain redistribution occurs along the LM wires, causing localized narrowing of LM channels. Such LM channel narrowing induced rapid increase in electrical resistance and thus the enhancement in sensitivity. Inspired by the simulation results, we further explore the sensitivity enhancement of the strain sensor by increasing the SiO$_2$ particle size to 0.6 mm, which is close to the width of the LM wires (0.9 mm). At large strains, significant stress concentration could be induced around the particles, and because of the blockage of the conductive path around the particles, rapid increase in effective resistance and thus gauge factor could be achieved. As shown in Figure 3c, the GF of the LM strain sensor using 0.6 mm SiO$_2$ particles increases from 5.72 between 0 and 100% strain to 11.63 between 100% and 200% strain, and further to 23.91 between 200% and 300% strain, which is almost 10 times enhancement from pure LM.

Besides the high sensitivity, stability and durability are of great importance for practical applications of strain sensors[57,58]. Cyclic loading and unloading testing of our strain sensors at 100% strain were conducted, and the results are shown in Figs. 3e and 3f. As shown in Fig. 3e, strain sensors with different filler loadings show excellent reversibility and repeatability, with negligible hysteresis, due to the great elasticity of Ecoflex and flowability of LM-SiO$_2$ composites. Moreover, the electrical response of the strain sensors exhibites excellent stability during 100 stretching-releasing cyclic test under 100% strain (Figure 3f). Due to the excellent mechanical flexibility, high sensitivity at both small and large strains, and the extremely wide sensing range, the LM strain sensors can be used as a wearable device on human to monitor subtle and large motions at different locations in real time. The LM strain sensors are attached to the eye, neck, fingers, and knees of the human body to detect various human motions (Figures 4a-4d). Not only the subtle muscle movements induced by micro-expression can be decoded from the analysis of the measured piezoresistive signals, but also the vigorous bending and releasing of the knee joint could be precisely recorded. Such demonstrated capabilities enable the LM sensor to be integrated with various objects to create application opportunities in intelligent soft robotic systems, interactive wearable electronics, and future human-machine interfaces.

In addition to strain sensing, the application of the LM sensor in pressure detection is also explored. Figure 4e exhibits the relative resistance change versus the pressure applied to the LM sensor. When the pressure exceeds a certain threshold, the LM sensor fails due to the collapse of conductive LM wires. The results indicate that the maximum pressure the sensor can withstand enhances from 696.3 kPa to 981.5 kPa as the SiO_2 weight fraction increases from 0% to 6% (inset of Figure 4e). The incorporation of SiO_2 particles can provide more resistance to counter the compressive force, resulting in improvement in the detectable pressure range. Figure 4f shows reversible loading-unloading behavior of the sensor with 6% SiO_2 particles for the applied pressure ranging from 100 kPa to 300 kPa. The relative resistance changes of the sensor under cyclic compressing-releasing tests of 100 kPa pressure for 100 cycles, as exhibited in Figure 4g, demonstrate excellent durability and repeatability. To illustrate the application in wearable electronics, the LM pressure sensor is attached to the bottom of a foot. Figure 4h shows that the LM sensor can detect and distinguish different motions of the foot, such as shaking leg, walking, running, and tiptoeing, and therefore could be used for gait identification.

2.3 Deep-Learning-Assisted Boxing Recognition

Precisely capturing the real-time strain and pressure information creates application opportunities for the LM sensor in boxing training, which can be utilized to provide sensory feedback for athletes to optimize the punching technique. As a proof of concept, the sensing arrays are printed and assembled onto every finger of a flexible tactile glove to decode fist clenching postures and impacting strengths (Figure 5a and Video S3). The bending angles of all five fingers can be obtained from the measured piezoresistive signals (Figure 5b), which could be used to distinguish between correct and incorrect fist clenching postures in real time. Compared with the relative resistance changes of the professional fist clenching method, incorrect fist gestures such as the valgus thumb, empty fist and invaginated little finger can be identified and distinguished using the real-time electrical signals (Figure 5c). In addition to the clenching posture, the strength of punching is also crucial to training and competition. The increase in the punching force leads to the enhanced sensing response (Figure 5d),

providing real-time visual feedback to trainees and coaches. Figure 5e shows that the sensory glove demonstrates excellent reversibility and reliability during punch-release cycles, without noticeable degradation in sensing signals.

Since the tactile glove is capable of decoding clenching postures and punching strength, it paves the way for the development of an intelligent boxing recognition system, in which various types of punching techniques[59,60] (e.g., jab, swing, uppercut, and combination punches, Figure 6a) can be distinguished in real time. For a unique demonstration towards the future application in sports training, the smart tactile glove is worn by a boxer to evaluate its recognition capability aided by the deep-learning algorithm. A convolutional neural network (CNN) architecture of the intelligent boxing system (Figure 6b) is proposed to achieve precise identification boxing punches. The whole data (containing 150 sets, 30 sets for each punch) are divided into a training set (90%) and a testing set (10%) to train the CNN model. Given the complexity of the sensing signals acquired from five different fingers in different punches (Figure 6c), only the real-time resistance change of the middle finger is used (Figure 6d) to simplify the analysis. The confusion map of the classified result indicates that the boxing recognition accuracy of the five punches can reach 90.5% (Figures 6e and 6f). This work clearly demonstrates the potential of printable liquid metal sensors in smart sport-training, human-machine interface, and humanoid robotics.

3. CONCLUSION

In summary, we have demonstrated a printable LM sensor with high sensitivity and excellent mechanical properties, via effective rheological modification of LM and strain redistribution mechanics tuned by SiO_2 particles. The incorporation of SiO_2 micro-particles increases the elastic modulus, viscous modulus, yield stress, and viscosity of LM, which enables rapidly customizable and scalable fabrication of soft electronics based on modified LMs through 3D printing. The inclusion of SiO_2 particles in LM leads to enhanced sensitivity at large tensile strains (the GF is 5.72 for strain range between 0 and 100%, 11.36 for 100-200%, and 23.91 for 200-300%) due to strain redistribution mechanics within the conductive LM wires, and superior mechanical

robustness to endure extreme pressure (i.e., 0.9 MPa). As a proof-of-concept demonstration, the multifunctional sensor is integrated onto a tactile glove to decode the clenching posture and hitting strength in boxing training. This tactile glove is shown to be able to identify different boxing punches (ab, swing, uppercut, and combination punches) with a recognition accuracy of 90.5%, assisted by a deep learning algorithm. The excellent combination of mechanical and electrical properties and demonstration in wearable systems promise great potential of the LM sensors in a wide variety of applications, such as smart sport-training, robotic operation, and human-machine interface.

4. METHODS

4.1 Material preparation

The eutectic metal alloy was synthesized by mixing gallium (75%) and indium (25%) (eGaIn, Sigma-Aldrich). It maintains liquid state at room temperature (15.7°C melting point). SiO_2 micro-particles (40 μm diameter, and 6μm diameter, Sigma-Aldrich) composing 0, 1, 3.5, 6, and 20 wt% were mixed into the eGaIn. The mixtures were stirred in the air at room temperature with 500 rpm for 2 min and 2000 rpm (vigorously stirred) for 8 min. After stirring, the mixtures containing eGaIn and uniformly distributed SiO_2 particle were obtained.

4.2 Rheological property test

The rheological characterization was performed using an Anton Paar Physica MCR 301 setup. The rheometer was equipped with a Peltier plate and parallel plate geometry of 25 mm diameter. All the tests were carried out at 25°C.

(1) Preshear for 120 s at 1 s^{-1} to eliminate loading history.

(2) A frequency sweep at 0.5% strain from 0.1 to 500 rad s^{-1} was used to determine elastic (G′) and viscous modulus (G″) of the composites.

(3) An amplitude sweep at 1 rad s^{-1} from 0.05 to 1000% strain was used to determine the linear viscoelastic region of the composites as well as two versions of oscillation yield stress (σ_y).

(4) A flow sweep from 0.01 to 10 s^{-1} was used to determine the shear rate

dependent viscosity (η) of the material.

4.3 FEA simulation

To investigate the mechanical deformation of the LM sensors, finite element analysis (FEA) was performed using ABAQUS. The Ecoflex and LM were modeled as Yeoh and Neo-Hookean hyperelastic materials using three-dimensional (3D) hybrid stress elements (C3D8H). The uniformly distributed SiO_2 particles were assembled into the LM wires by embedding constraints. SiO_2 particles were modeled using elastic isotropic material with 3D stress elements (C3D8R), with a Young's modulus of 76 GPa and a Poisson's ratio of 0.3. The coefficients C_{10}, C_{20}, and C_{30} were 0.0104 MPa, 0.0072 MPa, and 0.012 MPa for Ecoflex, by fitting experimental data from uniaxial tensile test (Figure S11). The coefficient of LM is set as C_{10} =0.5 kPa based on the shear modulus of 1 kPa.

4.4 3D structure printing

The composites with 1wt.% 6 μm SiO_2 particles were used to print complicated 3D structures utilizing a commercial modular 3D printer (Hydra 640 from Hyrel 3D, Figure S11). The syringe extrusion head on the printer was from a regular 10 ml syringe and the syringe plunger was precisely controlled by a linear motor. Nozzles with diameters 15 and 22 Ga were used to print star and sensor shapes, respectively. The one-layer star and four-layer star were printed by dispensing the composites layer by layer at a printing speed of 10 mm s^{-1} through a 15 Ga nozzle. The height of each layer was 0.7 mm. Besides, we directly printed strain sensors on a tactile glove over the first knuckle regions of each finger. Each sensor was 0.6 mm wide and 20 mm long, which was printed using a 22 Ga nozzle and a printing speed of 10 mm/s.

4.5 Fabrication and characterization of the sensors

The Ecoflex (a 1:1 mixture of Ecoflex part A and part B, Ecoflex Supersoft 0030, smooth-on, Inc.) substrate was coated on the glass by spin coating (1500 rpm for 30 s) and curing at 80°C for 30 min. The LM-SiO_2 composite wires were fabricated by printing onto the substrate. After the copper wires were attached to the printed LM wires, another Ecoflex encapsulation layer was coated on the top and cured at 80°C for 30 min. The sample was cut into strips (40 mm × 20 mm × 1 mm) and carefully peeled off

of the glass to obtain the sensors. To characterize the electrical response, the sensing signals from the sensors were obtained using a semiconductor parameter analyzer (4200-SCS, Keithley).

4.6 Mechanical test

The tension and compression tests were carried out using an Instron mechanical testing system (Instron LEGEND2345). The speed of the tensile test and tensile cyclic test were both 240 mm/min. Tensile cycling tests were performed 100 times under 100% strain. The speed of the compression test and compression cyclic test were both 2 mm/min. Compression cycling tests were carried out 100 times under 100 kPa pressure.

REFERENCES

(1) Lee, S.; Byun, S.; Kim, C. Y.; Cho, S.; Park, S.; Sim, J. Y.; Jeong, J. Beyond Human Touch Perception: An Adaptive Robotic Skin Based on Gallium Microgranules for Pressure Sensory Augmentation. *Adv. Mater.* **2022**, e2204805.

(2) Lee, G.; Lee, Y. R.; Kim, H.; Kwon, D. A.; Kim, H.; Yang, C.; Choi, S. Q.; Park, S.; Jeong, J.; Park, S. Rapid Meniscus-Guided Printing of Stable Semi-Solid-State Liquid Metal Microgranular-Particle for Soft Electronics. *Nat. Commun.* **2022**, 13 (1), 2643.

(3) Zhao, R.; Guo, R.; Xu, X.; Liu, J. A Fast and Cost-Effective Transfer Printing of Liquid Metal Inks for Three-Dimensional Wiring in Flexible Electronics. *ACS Appl. Mater. Interfaces* **2020**, 12 (32), 36723-36730.

(4) Zhou, L.; Gao, Q.; Zhan, J.; Xie, C.; Fu, J.; He, Y. Three-Dimensional Printed Wearable Sensors with Liquid Metals for Detecting the Pose of Snakelike Soft Robots. *ACS Appl. Mater. Interfaces* **2018**, 10 (27), 23208-23217.

(5) Yuan, B.; Zhao, C.; Sun, X.; Liu, J. Lightweight Liquid Metal Entity. *Adv. Funct. Mater.* **2020**, 30 (14), 1910709.

(6) Qiu, Y.; Wang, C.; Lu, X.; Wu, H.; Ma, X.; Hu, J.; Qi, H.; Tian, Y.; Zhang, Z.; Bao, G.; Chai, H.; Song, J.; Liu, A. A Biomimetic Drosera Capensis with Adaptive Decision−Predation Behavior Based on Multifunctional Sensing and Fast Actuating Capability. *Adv. Funct. Mater.* **2022**, 32 (13), 2110296.

(7) Liu, Z.; Qi, D.; Hu, G.; Wang, H.; Jiang, Y.; Chen, G.; Luo, Y.; Loh, X. J.; Liedberg, B.; Chen, X. Surface Strain Redistribution on Structured Microfibers to Enhance Sensitivity of Fiber-Shaped Stretchable Strain Sensors. *Adv. Mater.* **2018**, 30 (5), 1704229.

(8) Yamamoto, Y.; Harada, S.; Yamamoto, D.; Honda, W.; Arie, T.; Akita, S.; Takei, K. Printed Multifunctional Flexible Device with an Integrated Motion Sensor for Health Care Monitoring. *Sci. Adv.* **2016**, 2 (11), e1601473.

(9) Han, S.; Peng, H.; Sun, Q.; Venkatesh, S.; Chung, K.; Lau, S. C.; Zhou, Y.; Roy, V. A. L. An Overview of the Development of Flexible Sensors. *Adv. Mater.* **2017**, 29 (33), 1700375.

(10) Shi, C.; Zou, Z.; Lei, Z.; Zhu, P.; Zhang, W.; Xiao, J. Heterogeneous Integration of Rigid, Soft, and Liquid Materials for Self-Healable, Recyclable, and Reconfigurable Wearable Electronics. *Sci. Adv.* **2020**, 6 (45), eabd0202.

(11) Dickey, M. D. Emerging Applications of Liquid Metals Featuring Surface Oxides. *ACS Appl. Mater. Interfaces* **2014**, 6 (21), 18369-18379.

(12) Dickey, M. D. Stretchable and Soft Electronics Using Liquid Metals. *Adv. Mater.* **2017**, 29 (27), 1606425.

(13) Shan, W.; Lu, T.; Majidi, C. Soft-Matter Composites with Electrically Tunable Elastic Rigidity. *Smart Mater. Struct.* **2013**, 22 (8), 85001-85005.

(14) Cheng, S.; Rydberg, A.; Hjort, K.; Wu, Z. Liquid Metal Stretchable Unbalanced Loop Antenna. *Appl. Phys. Lett.* **2009**, 94 (14), 144103.

(15) Chen, J.; Zhang, J.; Luo, Z.; Zhang, J.; Li, L.; Su, Y.; Gao, X.; Li, Y.; Tang, W.; Cao, C.; Liu, Q.; Wang, L.; Li, H. Superelastic, Sensitive, and Low Hysteresis Flexible Strain Sensor Based on Wave-Patterned Liquid Metal for Human Activity Monitoring. *ACS Appl. Mater. Interfaces* **2020**, 12 (19), 22200-22211.

(16) Wu, H. P.; Qi, H. C.; Wang, X.; Qiu, Y.; Shi, K. Q.; Zhang, H. J.; Zhang, Z.; Zhang, W. A.; Tian, Y. Stretchable, Sensitive, Flexible Strain Sensor Incorporated with Patterned Liquid Metal on Hydrogel

for Human Motion Monitoring and Human-Machine Interaction. *J. Mater. Chem. C* **2022**, 10 (21), 8206-8217.

(17) Wang, Q.; Yu, Y.; Liu, J. Preparations, Characteristics and Applications of the Functional Liquid Metal Materials. *Adv. Eng. Mater.* **2018**, 20 (5), 1700781.

(18) Xu, Q.; Oudalov, N.; Guo, Q.; Jaeger, H. M.; Brown, E. Effect of Oxidation on the Mechanical Properties of Liquid Gallium and Eutectic Gallium-Indium. *Phys. Fluids* **2012**, 24 (6), 63101.

(19) Ladd, C.; So, J.; Muth, J.; Dickey, M. D. 3D Printing of Free Standing Liquid Metal Microstructures. *Adv. Mater.* **2013**, 25 (36), 5081-5085.

(20) Harada, S.; Arie, T.; Akita, S.; Takei, K. Highly Stable Liquid-Solid Metal Contact Toward Multilayered Detachable Flexible Devices. *Adv. Electron. Mater.* **2015**, 1 (7), 1500080.

(21) Chen, X.; Wan, H.; Guo, R.; Wang, X.; Wang, Y.; Jiao, C.; Sun, K.; Hu, L. A Double-Layered Liquid Metal-Based Electrochemical Sensing System on Fabric as a Wearable Detector for Glucose in Sweat. *Microsyst. Nanoeng.* **2022**, 8 (1), 48.

(22) Zhang, Y.; Zheng, N.; Cao, Y.; Wang, F.; Wang, P.; Ma, Y.; Lu, B.; Hou, G.; Fang, Z.; Liang, Z.; Yue, M.; Li, Y.; Chen, Y.; Fu, J.; Wu, J.; Xie, T.; Feng, X. Climbing-Inspired Twining Electrodes Using Shape Memory for Peripheral Nerve Stimulation and Recording. *Sci. Adv.* **2019**, 5 (4), w1066.

(23) Boutry, C. M.; Negre, M.; Jorda, M.; Vardoulis, O.; Chortos, A.; Khatib, O.; Bao, Z. A Hierarchically Patterned, Bioinspired E-Skin Able to Detect the Direction of Applied Pressure for Robotics. *Sci. Robot.* **2018**, 3 (24), eaau6914.

(24) Ren, W.; Sun, Y.; Zhao, D. L.; Aili, A.; Zhang, S.; Shi, C. Q.; Zhang, J. L.; Geng, H. Y.; Zhang, J.; Zhang, L. X.; Xiao, J. L.; Yang, R. G. High-performance Wearable Thermoelectric Generator with Self-healing, Recycling and Lego-like Reconfiguring Capabilities. *Sci. Adv.* **2021**, 7 (7), eabe0586.

(25) Zhu, P. C.; Shi, C. Q.; Wang, Y. L.; Wang, Y. L.; Yu, Y. D.; Wang, Y.; Deng, Y.; Xiao,J. Recyclable, Healable and Stretchable High-power Thermoelectric Generator. *Adv. Energy. Mater.* **2021**, 11 (25), 2100920.

(26) Zhang, J.; Yao, H.; Mo, J.; Chen, S.; Xie, Y.; Ma, S.; Chen, R.; Luo, T.; Ling, W.; Qin, L.; Wang, Z.; Zhou, W. Finger-Inspired Rigid-Soft Hybrid Tactile Sensor with Superior Sensitivity at High Frequency. *Nat. Commun.* **2022**, 13 (1), 5076.

(27) Won, S. M.; Wang, H.; Kim, B. H.; Lee, K.; Jang, H.; Kwon, K.; Han, M.; Crawford, K. E.; Li, H.; Lee, Y.; Yuan, X.; Kim, S. B.; Oh, Y. S.; Jang, W. J.; Lee, J. Y.; Han, S.; Kim, J.; Wang, X.; Xie, Z.;

Zhang, Y.; Huang, Y.; Rogers, J. A. Multimodal Sensing with a Three-Dimensional Piezoresistive Structure. *ACS Nano* **2019**, 13 (10), 10972-10979.

(28) Shi, C. Q.; Zhao, Y.; Zhu, P. C.; Xiao, J. L.; Nie, G. H. Highly Stretchable and Rehealable Wearable Strain Sensor Based on Dynamic Covalent Thermoset and Liquid Metal. *Smart Mater Struct*. **2021**, 30 (10), 105001.

(29) Byun, S. H.; Yun, J. H.; Heo, S. Y.; Shi, C. Q.; Lee, G. J.; K.-C. Agno, K. C.; Jang, K. I.; Xiao, J. L.; Song, Y. M.; Jeong, J. W. Self-Cooling Gallium-Based Transformative Electronics with a Radiative Cooler for Reliable Stiffness Tuning in Outdoor Use. *Sci. Adv.* **2022**, 9 (24), 2022549.

(30) He, K.; Liu, Y.; Wang, M.; Chen, G.; Jiang, Y.; Yu, J.; Wan, C.; Qi, D.; Xiao, M.; Leow, W. R.; Yang, H.; Antonietti, M.; Chen, X. An Artificial Somatic Reflex Arc. *Adv. Mater.* **2019**, 32 (4), 1905399.

(31) Chen, G.; Yang, Z.; Wang, W.; Bi, L.; Chen, L.; Peng, Y.; Ye, C. Electrothermal Actuators with Ultrafast Response Speed and Large Deformation. *Adv. Intell. Syst.* **2020**, 2 (8), 2000036.

(32) Zhou, H.; Zhang, Y.; Qiu, Y.; Wu, H.; Qin, W.; Liao, Y.; Yu, Q.; Cheng, H. Stretchable Piezoelectric Energy Harvesters and Self-Powered Sensors for Wearable and Implantable Devices. *Biosens. Bioelectron.* **2020**, 168, 112569.

(33) Qiu, Y.; Tian, Y.; Sun, S.; Hu, J.; Wang, Y.; Zhang, Z.; Liu, A.; Cheng, H.; Gao, W.; Zhang, W.; Chai, H.; Wu, H. Bioinspired, Multifunctional Dual-Mode Pressure Sensors as Electronic Skin for Decoding Complex Loading Processes and Human Motions. *Nano Energy* **2020**, 78, 105337.

(34) Wang, C.; Linghu, C.; Nie, S.; Li, C.; Lei, Q.; Tao, X.; Zeng, Y.; Du Y; Zhang, S.; Yu, K.; Jin, H.; Chen, W.; Song, J. Programmable and Scalable Transfer Printing with High Reliability and Efficiency for Flexible Inorganic Electronics. *Sci. Adv.* **2020**, 6 (25), b2393.

(35) Qiu, Y.; Sun, S.; Wang, X.; Shi, K.; Wang, Z.; Ma, X.; Zhang, W.; Bao, G.; Tian, Y.; Zhang, Z.; Ding, H.; Chai, H.; Liu, A.; Wu, H. Nondestructive Identification of Softness Via Bioinspired Multisensory Electronic Skins Integrated on a Robotic Hand. *npj. Flex. Electron.* **2022**, 6 (1), 1-10.

(36) Cui, Z.; Wang, W.; Guo, L.; Liu, Z.; Cai, P.; Cui, Y.; Wang, T.; Wang, C.; Zhu, M.; Zhou, Y.; Liu, W.; Zheng, Y.; Deng, G.; Xu, C.; Chen, X. Haptically Quantifying Young's Modulus of Soft Materials Using a Self‑Locked Stretchable Strain Sensor. *Adv. Mater.* **2022**, 34 (25), 2104078.

(37) Jeong, Y. R.; Kim, J.; Xie, Z.; Xue, Y.; Won, S. M.; Lee, G.; Jin, S. W.; Hong, S. Y.; Feng, X.; Huang, Y.; Rogers, J. A.; Ha, J. S. A Skin-Attachable, Stretchable Integrated System Based on Liquid Gainsn for Wireless Human Motion Monitoring with Multi-Site Sensing Capabilities. *NPG Asia Mater.*

2017, 9 (10), e443.

(38) Tang, J.; Zhao, X.; Li, J.; Guo, R.; Zhou, Y.; Liu, J. Gallium-Based Liquid Metal Amalgams: Transitional-State Metallic Mixtures (TransM² ixes) with Enhanced and Tunable Electrical, Thermal, and Mechanical Properties. *ACS Appl. Mater. Interfaces* **2017**, 9 (41), 35977-35987.

(39) Xiong, M.; Gao, Y.; Liu, J. Fabrication of Magnetic Nano Liquid Metal Fluid through Loading of Ni Nanoparticles Into Gallium or its Alloy. *J. Magn. Magn. Mater.* **2014**, 354, 279-283.

(40) Tang, J.; Zhao, X.; Li, J.; Zhou, Y.; Liu, J. Liquid Metal Phagocytosis: Intermetallic Wetting Induced Particle Internalization. *Adv. Sci.* **2017**, 4 (5), 1700024.

(41) Carle, F.; Bai, K.; Casara, J.; Vanderlick, K.; Brown, E. Development of Magnetic Liquid Metal Suspensions for Magnetohydrodynamics. *Phys. Rev. Fluids* **2017**, 2 (1), 013301.

(42) Daalkhaijav, U.; Yirmibesoglu, O. D.; Walker, S.; Mengüç, Y. Rheological Modification of Liquid Metal for Additive Manufacturing of Stretchable Electronics. *Adv. Mater. Technol.* **2018**, 3 (4), 1700351.

(43) Syed, N.; Zavabeti, A.; Mohiuddin, M.; Zhang, B.; Wang, Y.; Datta, R. S.; Atkin, P.; Carey, B. J.; Tan, C.; van Embden, J.; Chesman, A. S. R.; Ou, J. Z.; Daeneke, T.; Kalantar-zadeh, K. Sonication-Assisted Synthesis of Gallium Oxide Suspensions Featuring Trap State Absorption: Test of Photochemistry. *Adv. Funct. Mater.* **2017**, 27 (43), 1702295.

(44) Boley, J. W.; White, E. L.; Kramer, R. K. Mechanically Sintered Gallium-Indium Nanoparticles. *Adv. Mater.* **2015**, 27 (14), 2355-2360.

(45) Lu, Y.; Hu, Q.; Lin, Y.; Pacardo, D. B.; Wang, C.; Sun, W.; Ligler, F. S.; Dickey, M. D.; Gu, Z. Transformable Liquid-Metal Nanomedicine. *Nat. Commun.* **2015**, 6, 10066.

(46) Amjadi, M.; Kyung, K.; Park, I.; Sitti, M. Stretchable, Skin-Mountable, and Wearable Strain Sensors and their Potential Applications: A Review. *Adv. Funct. Mater.* **2016**, 26 (11), 1678-1698.

(47) Qiu, A.; Li, P.; Yang, Z.; Yao, Y.; Lee, I.; Ma, J. A Path Beyond Metal and Silicon:Polymer/Nanomaterial Composites for Stretchable Strain Sensors. *Adv. Funct. Mater.* **2019**, 29 (17), 1806306.

(48) Boley, J. W.; White, E. L.; Chiu, G. T. C.; Kramer, R. K. Direct Writing of Gallium-Indium Alloy for Stretchable Electronics. *Adv. Funct. Mater.* **2014**, 24 (23), 3501-3507.

(49) Dickey, M. D.; Chiechi, R. C.; Larsen, R. J.; Weiss, E. A.; Weitz, D. A.; Whitesides, G. M. Eutectic Gallium-Indium (Egain): A Liquid Metal Alloy for the Formation of Stable Structures in Microchannels at Room Temperature. *Adv. Funct. Mater.* **2008**, 18 (7), 1097-1104.

(50) Wang, Q.; Yu, Y.; Yang, J.; Liu, J. Fast Fabrication of Flexible Functional Circuits Based on Liquid Metal Dual-Trans Printing. *Adv. Mater.* **2015**, 27 (44), 7109-7116.

(51) Chossat, J.; Park, Y.; Wood, R. J.; Duchaine, V. A Soft Strain Sensor Based on Ionic and Metal Liquids. *IEEE Sens. J.* **2013**, 13 (9), 3405-3414.

(52) Choi, J.; Han, C.; Cho, S.; Kim, K.; Ahn, J.; Del Orbe, D.; Cho, I.; Zhao, Z. J.; Oh, Y. S.; Hong, H.; Kim, S. S.; Park, I. Customizable, Conformal, and Stretchable 3D Electronics Via Predistorted Pattern Generation and Thermoforming. *Sci. Adv.* **2021**, 7 (42), eabj0694.

(53) Muth, J. T.; Vogt, D. M.; Truby, R. L.; Mengüç, Y.; Kolesky, D. B.; Wood, R. J.; Lewis, J. A. Embedded 3D Printing of Strain Sensors within Highly Stretchable Elastomers. *Adv. Mater.* **2014**, 26 (36), 6307-6312.

(54) Song, Z.; Li, W.; Bao, Y.; Han, F.; Gao, L.; Xu, J.; Ma, Y.; Han, D.; Niu, L. Breathable and Skin-Mountable Strain Sensor with Tunable Stretchability, Sensitivity, and Linearity Via Surface Strain Delocalization for Versatile Skin Activities´Recognition. *ACS Appl. Mater. Interfaces* **2018**, 10 (49), 42826-42836.

(55) Kim, I.; Woo, K.; Zhong, Z.; Ko, P.; Jang, Y.; Jung, M.; Jo, J.; Kwon, S.; Lee, S.; Lee, S.; Youn, H.; Moon, J. A Photonic Sintering Derived Ag Flake/Nanoparticle-Based Highly Sensitive Stretchable Strain Sensor for Human Motion Monitoring. *Nanoscale* **2018**, 10 (17), 7890-7897.

(56) Shi, X.; Liu, S.; Sun, Y.; Liang, J.; Chen, Y. Lowering Internal Friction of 0D-1D-2D Ternary Nanocomposite-Based Strain Sensor by Fullerene to Boost the Sensing Performance. *Adv. Funct. Mater.* **2018**, 28 (22), 1800850.

(57) Shi, C.; Zou, Z.; Lei, Z.; Zhu, P.; Nie, G.; Zhang, W.; Xiao, J. Stretchable, Rehealable, Recyclable, and Reconfigurable Integrated Strain Sensor for Joint Motion and Respiration Monitoring. *Research* **2021**, 2021, 1-14.

(58) Liao, X. Q.; Zhang, Z.; Kang, Z.; Gao, F. F.; Liao, Q. L.; Zhang, Y. Ultrasensitive and Stretchable Resistive Strain Sensors Designed for Wearable Electronics. *Mater. Horizons* **2017**, 4 (3), 502-510.

(59) Menzel, T.; Potthast, W. Validation of a Novel Boxing Monitoring System to Detect and Analyse the Centre of Pressure Movement on the Boxer´s Fist. *Sensors* **2021**, 21 (24), 8394.

(60) Ma, Z.; Meng, B.; Wang, Z.; Yuan, C.; Liu, Z.; Zhang, W.; Peng, Z. A Triboelectric-Piezoresistive Hybrid Sensor for Precisely Distinguishing Transient Processes in Mechanical Stimuli. *Nano Energy* **2020**, 78, 105216.
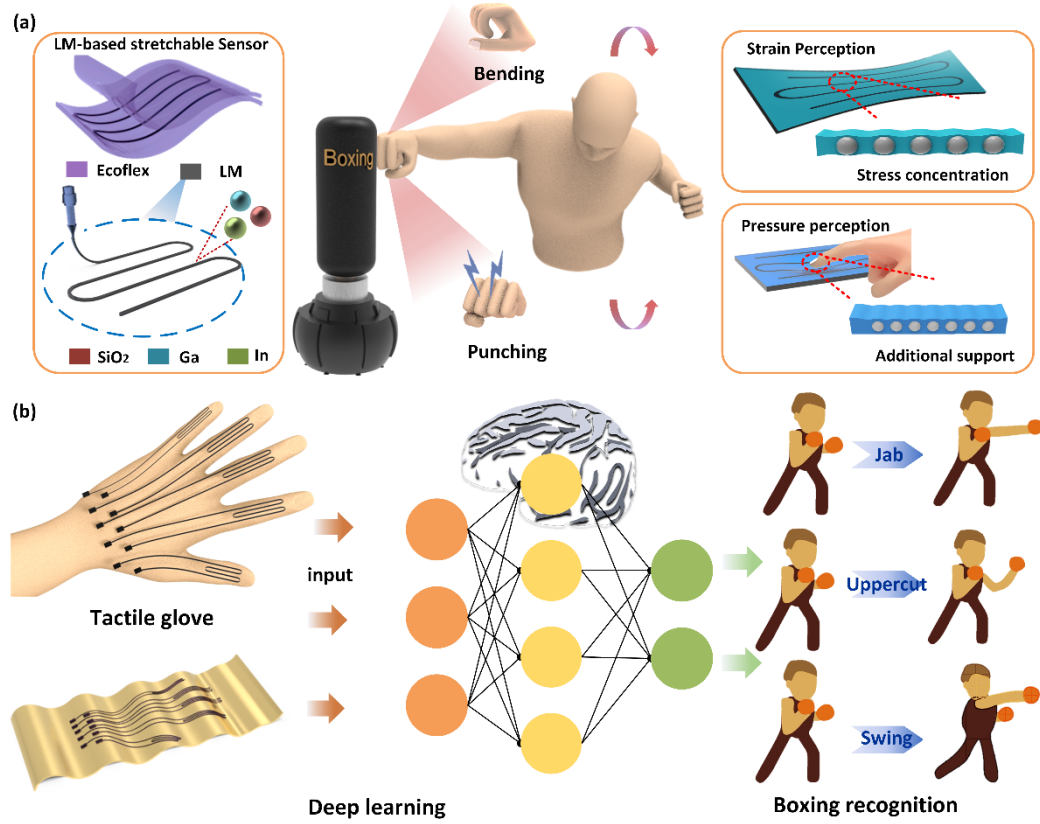
Figure 1. Printable liquid metal sensors and tactile glove with boxing recognition capability.

(a) Schematic illustrations of the structure of the printable LM sensors integrated on boxing gloves. The strain redistribution mechanics and enhanced pressure resistance due to SiO_2 particles in LM render the flexible sensors high sensitivity and robustness, thus perceiving strain and pressure stimuli during bending and punching process in the boxing sport. **(b)** The multisensory feedback enables the tactile glove to achieve boxing recognition, assisted with a deep learning algorithm.

Figure 2. Rheology test and 3D printing of LM-SiO₂ composites. **(a)** The average elastic modulus and **(b)** yield stress are derived from the oscillation amplitude sweep. **(c)** The yield stress is derived from the stress growth test. **(d)** The viscosity at a shear rate of 10 s⁻¹ is derived from the flow sweep test. Photographs of 3D Printed liquid metal structures: **(e)** one-layer star and **(f)** four-layer star.
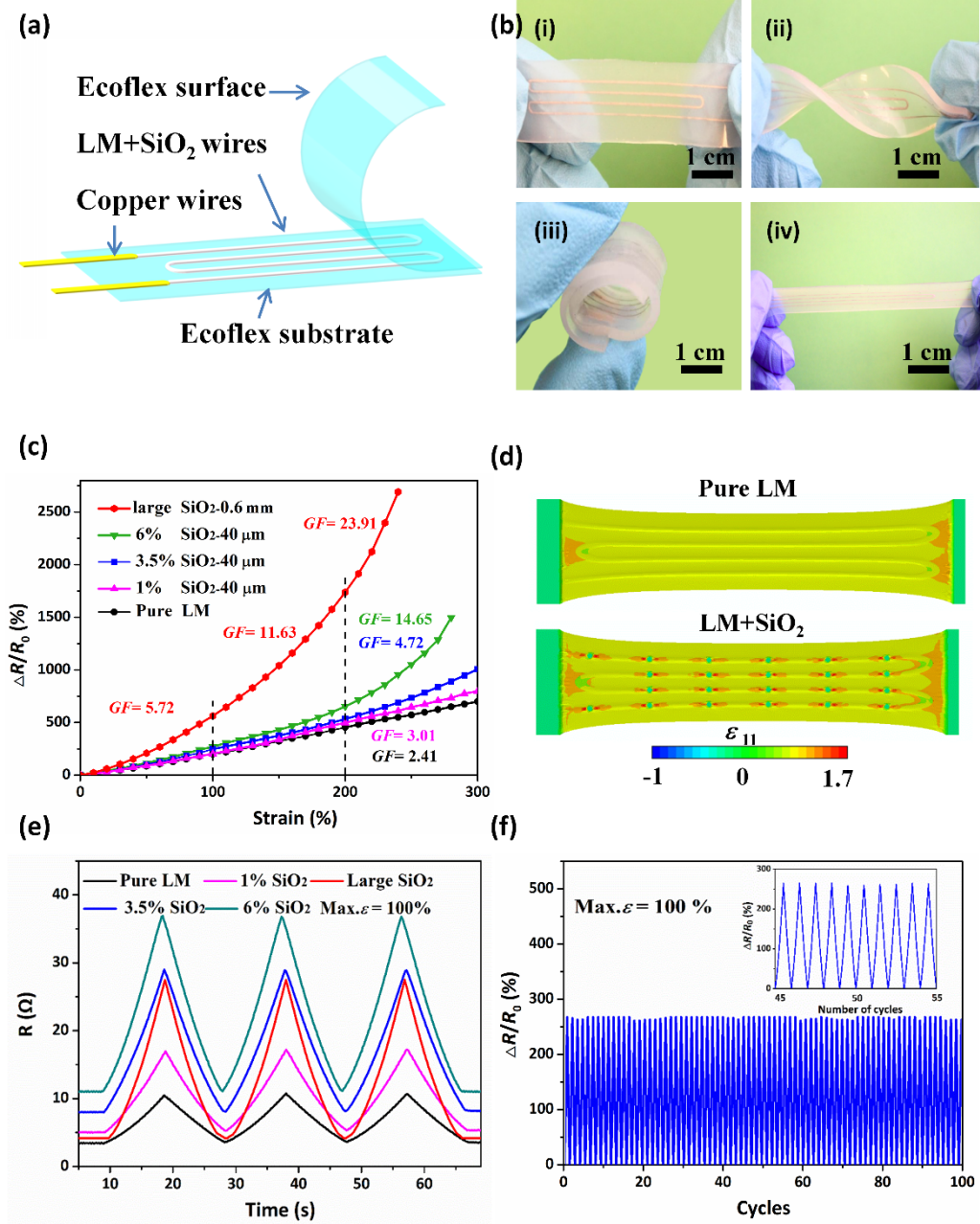
Figure 3. Strain sensing of the LM sensor. (a) Schematic illustration of the structure of the LM strain sensor. **(b)** Optical images of the sensor under different deformation modes: (i) initial state, (ii) twisted, (iii) rolled, and (iv) stretched. **(c)** Relative change of electrical resistance versus strain of the LM sensors with different SiO_2 filler loadings. **(d)** Mechanical simulation results of strain distributions within the LM sensors based on pure LM (top) and LM-SiO_2 composite (bottom) under 100% tensile strain. **(e)** Reversible loading-unloading behavior of the LM sensors with different SiO_2 filler loadings. **(f)** Relative resistance change during cyclic stretching-releasing test.
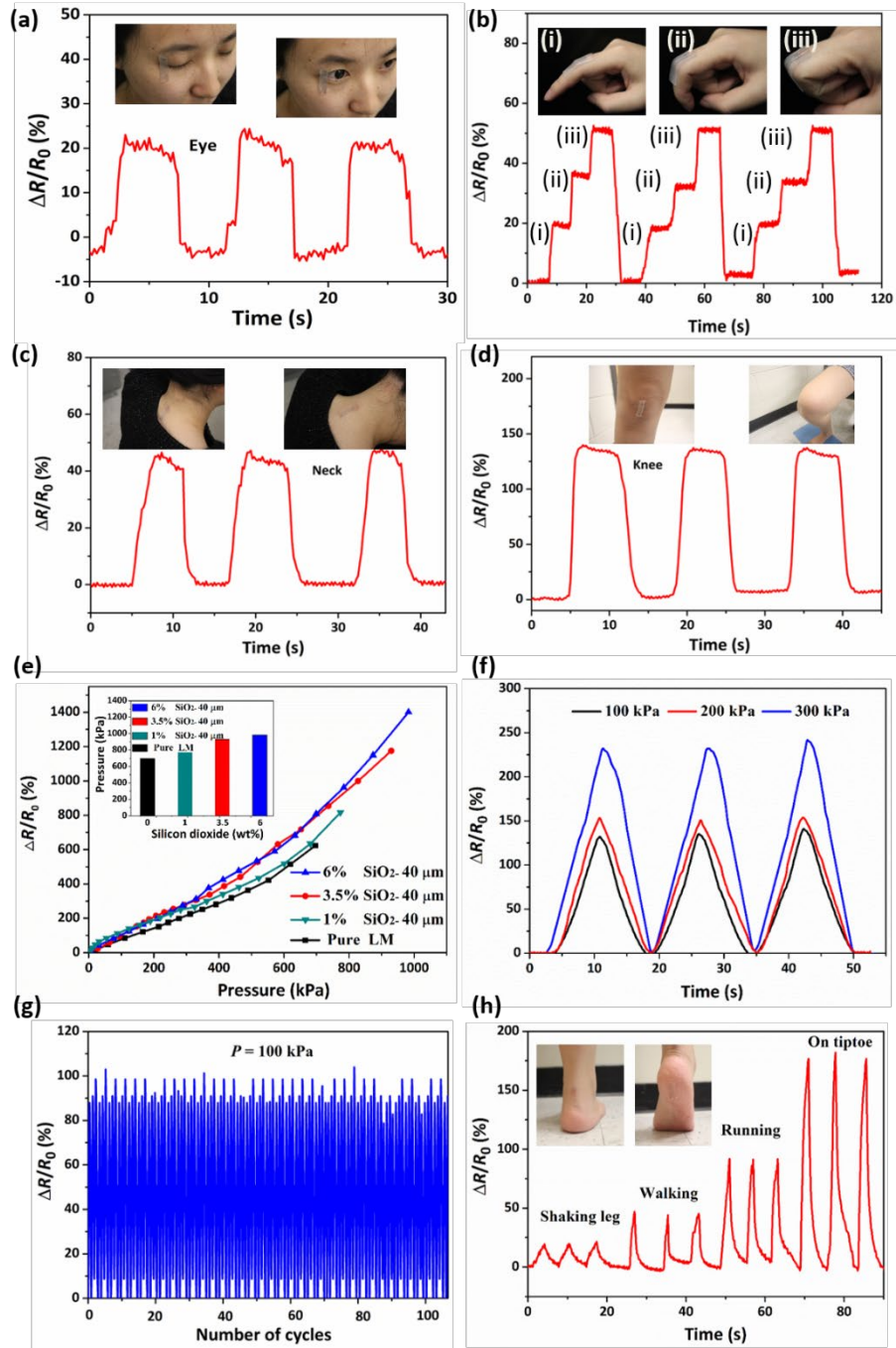
Figure 4. Real-time monitoring of various human motions using the LM strain and pressure sensors. Applications of the strain sensor as a human joint motion decoder in real time: **(a)** eye, **(b)** finger, **(c)** neck, and **(d)** knee. **(e)** Relative change of electrical resistance versus pressure of the LM pressure sensors with different SiO_2 filler loadings. **(f)** Reversible loading-unloading behavior of the sensors under 100 kPa, 200 kPa, and 300 kPa pressures. **(g)** Relative resistance change under cyclic compressing-releasing tests. **(h)** Application of the pressure sensor as a human plantar pressure decoder.
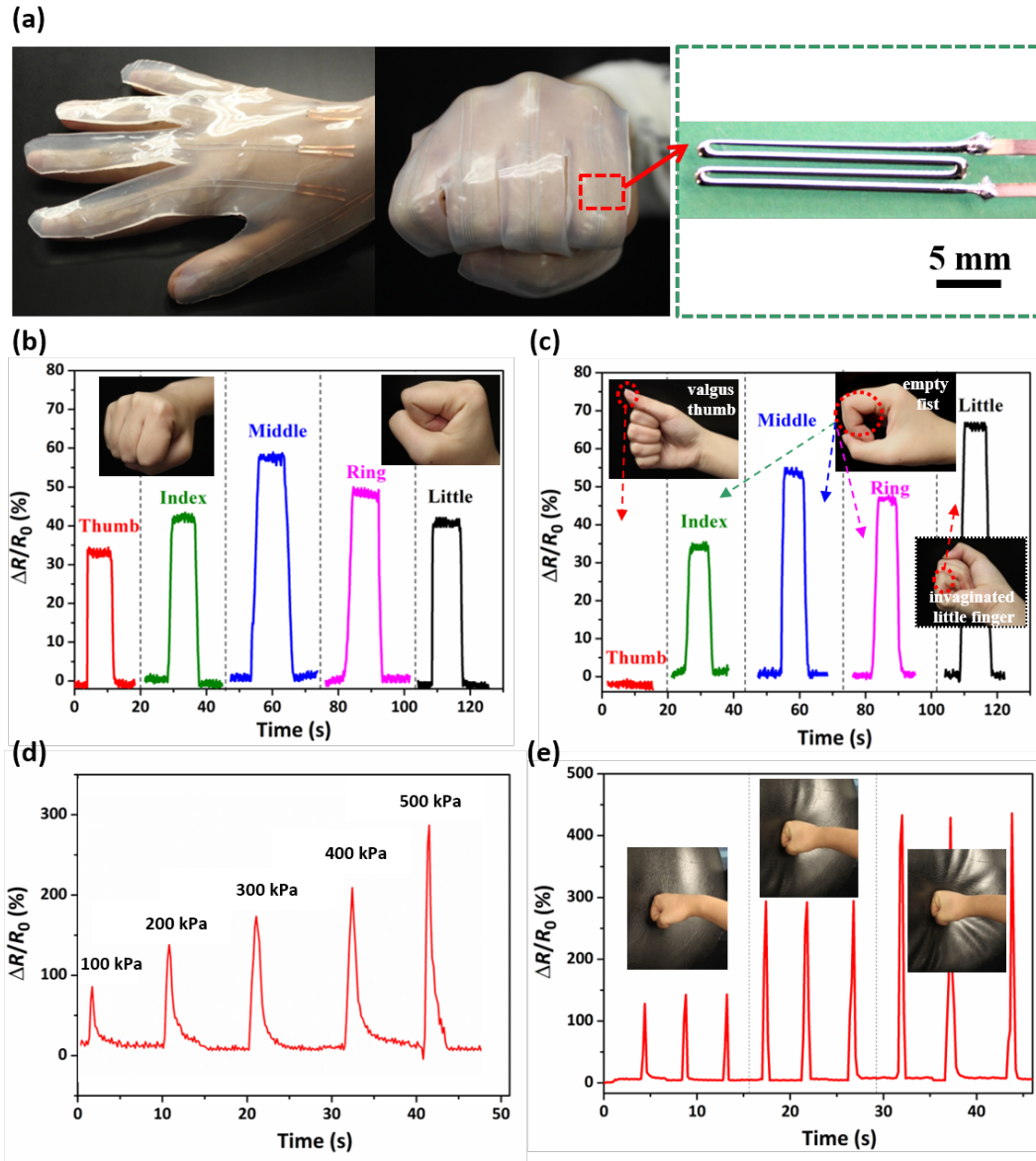
Figure 5. LM sensor for decoding the clenching posture and hitting strength of a punch in boxing training. **(a)** Photograph of an flexible tactile glove integrated with 3D-printed sensors. Relative resistance change of the sensors in response to the **(b)** correct and **(c)** wrong clenching postures. **(d)** The electrical signals of the sensor at increased pressures. **(e)** Relative resistance change of the sensor in response to various punching strength.
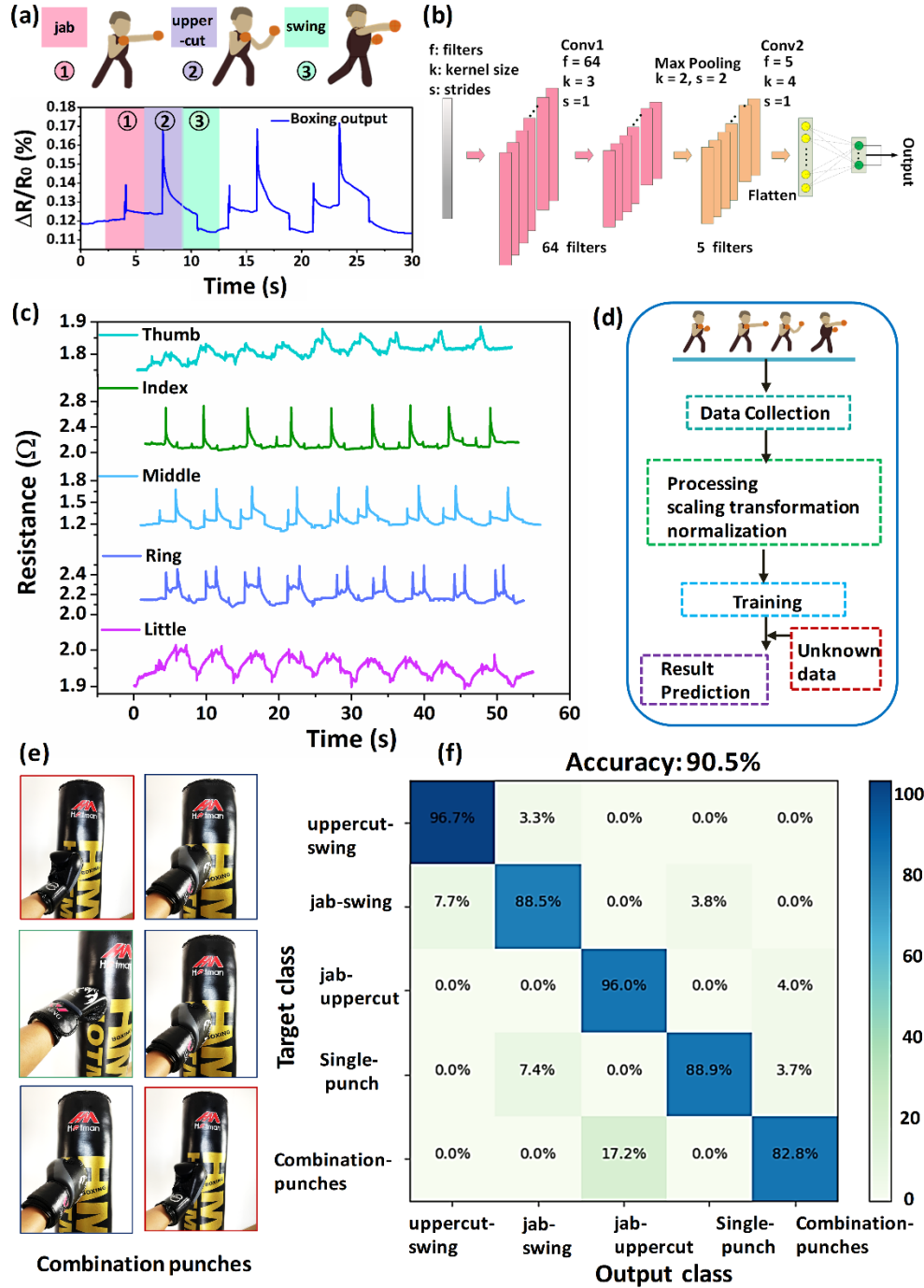
Figure 6. Boxing identification of tactile glove assisted with deep learning. (a) Schematics of three boxing punches and corresponding sensing signals. **(b)** The CNN architecture constructed for identifying boxing postures from tactile information input. **(c)** The excerpts of output resistance of five fingers corresponding to the jab, uppercut, and swing punches. **(d)** The process for training and real-time identification. **(e)** Photographs of combination punches used in the dataset. **(f)** Classification test confusion matrix of boxing recognition derived from the tactile glove.